Stabilization of standing waves through time-delay feedback

Michael Stich* and Alfonso Casal
Departamento de Matemática Aplicada, ETSAM, Universidad Politécnica de Madrid, Avenida Juan de Herrera 4, 28040 Madrid, Spain

Carsten Beta
Institut für Physik und Astronomie, Universität Potsdam, Karl-Liebknecht-Strasse 24/25, Haus 28, 14476 Potsdam, Germany
(Received 8 July 2013; published 17 October 2013)

Standing waves are studied as solutions of a complex Ginzburg-Landau equation subjected to local and global time-delay feedback terms. The onset is described as an instability of the uniform oscillations with respect to spatially periodic perturbations. The solution of the standing wave pattern is given analytically and studied through simulations.

DOI: 10.1103/PhysRevE.88.042910 PACS number(s): 82.40.Bj, 05.45.Gg

I. INTRODUCTION

The supercritical Hopf bifurcation is one of the simplest ways that a stationary state in a nonlinear system can undergo a transition to sustained oscillations. There, a small-amplitude limit cycle is born which already at onset displays a finite frequency. If we are considering a reaction-diffusion system, the dynamics of a system that undergoes such a bifurcation is described by the complex Ginzburg-Landau equation [1,2]. The primary solution of this system is the homogeneous periodic solution (uniform oscillations), corresponding to the limit cycle appearing at the Hopf bifurcation. However, the uniform oscillations in the spatially extended system may be unstable. The resulting states of spatiotemporal chaos appear if the Benjamin-Feir-Newell criterion $1 + \alpha\beta < 0$ is fulfilled, a phenomenon that is induced by the diffusive coupling and that is therefore genuine to a system with spatial degrees of freedom.

Considerable efforts have been made to understand this type of chaotic behavior and to apply methods to suppress this kind of turbulence and replace it with simpler, more regular dynamics. Consequently, control of chaotic states in nonlinear systems is a wide field of research that we cannot review here and we refer the reader to [3,4]. In the context of the reaction-diffusion systems, the introduction of forcing terms or global feedback terms have been shown to be efficient ways to control turbulence. To cite only one example, chemical turbulence can be suppressed by global time-delayed feedback [5,6] in the CO oxidation reaction on Pt(110) or in the photosensitive Belousov-Zhabotinsky reaction [7].

Global feedback methods, where a spatially independent quantity (or a spatial average of a space-dependent quantity) is coupled back to the system dynamics, have attracted much attention since in many cases the implementation in experiments is easier and the mathematical analysis simpler [4]. Nevertheless, local methods have gained interest in recent years since they allow to access other solutions of the systems in such diverse media as neurophysiological [8], cardiac [9], or semiconductor systems [10,11]. A local scheme with zero time delay was used in [12] to suppress spatiotemporal chaos in the CO oxidation system by the creation of localized wave sources (pacemakers).

The effect of local feedback on the complex Ginzburg-Landau equation (CGLE) was investigated by Socolar and co-workers [13,14]. Later, Silber and co-workers investigated a feedback scheme that included spatial shifts and in this way were able to stabilize traveling waves [15,16]. In electrochemical systems, nonlocal coupling arises naturally and the onset of pattern formation has been formulated in terms of a nonlocal CGLE [17–19], including the description of standing waves [18].

Feedback methods with an explicit time delay amplify the range of possibilities of control that can be applied to the system and provide the researcher with an additional adjustable parameter. On the level of the mathematical description, the model equations become delay differential equations [20]. One of the most important time-delay feedback schemes is due to Pyragas, who proposed to generate a control signal from the *difference* between the actual system state and a time-delayed one [21].

Motivated by previous work [22,23], we studied the CGLE subjected to a time-delay feedback with local and global terms [24–26] where each feedback term is of the Pyragas type. Extensive simulations showed the range of patterns that can be stabilized as a function of the local and global feedback terms [24]. If the feedback is global, uniform oscillations, the basic time-periodic solution of a system close to a Hopf bifurcation, can be stabilized for a large range of feedback parameters, while standing waves are found only in a small parameter area. As the contribution of the local feedback term becomes larger, the parameter regions increase where standing waves and—to a lesser extent—traveling waves are found. In [25], we studied the homogeneous periodic and the homogeneous stationary (amplitude death) solutions from an analytical point of view, performed linear stability analysis and derived the limiting curves of the stability regions. In [26], we proposed an analytic solution of standing waves for our model. In the present article, we show the derivation of this solution in detail, present simulations of standing waves, and compare the numerical with the analytical results. We

*Corresponding author: m.stich@aston.ac.uk; Present address: Non-linearity and Complexity Research Group, SEAS, Aston University, Aston Triangle, Birmingham B4 7ET, United Kingdom.

demonstrate that the agreement between our analytical and numerical findings is good and that the theory—in spite of a series of simplifications—describe the observed pattern very well.

This paper is organized as follows. In Sec. II, we introduce the model and describe briefly the basic solution, uniform oscillations. In Sec. III, we present the standing wave solution, including a pattern overview, analytic solution, and numerical simulations. We conclude the work in Sec. IV.

II. THE MODEL AND ITS BASIC SOLUTION

Reaction-diffusion systems can display various types of oscillatory dynamics. However, close to a supercritical Hopf bifurcation, all such systems are described by the CGLE [1,2],

$$\frac{\partial A}{\partial t} = (1 - i\omega)A - (1 + i\alpha)|A|^2 A + (1 + i\beta)\Delta A,$$

where A is the complex oscillation amplitude, ω the linear frequency parameter, α the nonlinear frequency parameter, β the linear dispersion coefficient, and Δ the Laplacian operator. For $1 + \alpha\beta < 0$ (the Benjamin-Feir-Newell criterion), the homogeneous periodic solution $A_u = e^{-i(\omega+\alpha)t}$ is unstable and a regime of spatiotemporal chaos is observed.

The CGLE for a one-dimensional medium with a combination of local and global time-delayed feedback has been introduced in Ref. [24] and reads

$$\begin{aligned} \frac{\partial A}{\partial t} &= (1 - i\omega)A - (1 + i\alpha)|A|^2 A + (1 + i\beta)\frac{\partial^2 A}{\partial x^2} + F, \\ F &= \mu e^{i\xi}\{m_l[A(x,t-\tau) - A(x,t)] \\ &\quad + m_g[\bar{A}(t-\tau) - \bar{A}(t)]\}, \end{aligned} \tag{1}$$

where

$$\bar{A}(t) = \frac{1}{L}\int_0^L A(x,t)\,dx$$

denotes the spatial average of A over a one-dimensional medium of length L. The parameter μ describes the feedback strength and ξ characterizes a phase shift between the feedback and the current dynamics of the system. The feedback has a local contribution F_l and a global one F_g,

$$\begin{aligned} F_l &= \mu m_l e^{i\xi}[A(x,t-\tau) - A(x,t)], \\ F_g &= \mu m_g e^{i\xi}[\bar{A}(t-\tau) - \bar{A}(t)]. \end{aligned} \tag{2}$$

If $m_l = 0$, the case of global time-delay feedback is retrieved [23].

As result of extensive simulations, many different spatiotemporal patterns have been identified in this system [24]. These include, but are not limited to, uniform oscillations, standing waves, traveling waves, amplitude death, and spatiotemporal chaos. The stabilization of uniform oscillations (homogeneous periodic solution) and amplitude death (homogeneous trivial solution) have been considered in [25]. Before discussing the standing wave solution, we introduce the homogeneous periodic solution. The solution of feedback-induced uniform oscillations is given by

$$A_0(t) = \rho_0 e^{-i\Omega t}. \tag{3}$$

It is a solution of Eq. (1) with the amplitude and frequency given by

$$\begin{aligned} \rho_0 &= \sqrt{1 + \mu(m_g + m_l)\chi_1}, \\ \Omega &= \omega + \alpha + \mu(m_g + m_l)(\alpha\chi_1 - \chi_2). \end{aligned} \tag{4}$$

Here, $\chi_{1,2}$ denote effective modulation terms that can be positive or negative. They arise from the feedback and hence depend on ξ and τ:

$$\begin{aligned} \chi_1 &= \cos(\xi + \Omega\tau) - \cos\xi, \\ \chi_2 &= \sin(\xi + \Omega\tau) - \sin\xi. \end{aligned} \tag{5}$$

In general, no explicit analytic solution for Eqs. (4) can be given because $\chi_{1,2}$ also depend on Ω. Nevertheless, the solution can be computed using root-finding algorithms, as done in [25].

III. STANDING WAVES

A. Pattern overview

In system (1), standing waves appear in parameter areas adjacent to regions where stable uniform oscillations are observed. In Fig. 1, we show typical space-time diagrams as μ is varied. The parameter set is chosen as in Refs. [24,25] such that in the absence of feedback, the system undergoes spatiotemporal chaos. For large μ, the feedback induces uniform oscillations [Fig. 1(a)]. Then, as μ is decreased, harmonic, small-amplitude standing waves set in [Fig. 1(b)]. As μ decreases further, the amplitude profile of these waves may show a period-2 behavior in space [Fig. 1(c)], before the standing waves start to "breathe" [Fig. 1(d)]. Finally, spatiotemporal chaos sets in [Fig. 1(e)]. In this paper, we describe the onset of standing waves in more detail. For standing waves, the (real) amplitude of the oscillation is modulated close to the corresponding value of uniform oscillations and is *constant* in time. In [26], we announced the standing wave solution, and here we describe the derivation and implications in more detail. Since close to onset, the amplitude of the modulation is small and its profile is harmonic, the onset of standing waves can be perceived as instability of the uniform solution with respect to space-dependent perturbations of wave number k_c.

B. Analytical solution

The stability analysis for uniform oscillations has been presented in detail in Ref. [25] and we just state that the uniform periodic solution becomes unstable with respect to standing waves with wavelength $2\pi/k_c$ when we have

$$\begin{aligned} &\lambda_1(k_c) = 0, \quad \partial_k\lambda_1(k_c) = 0, \quad \text{and} \\ &\lambda_2(k_c) = 0, \quad \text{with} \quad k_c \neq 0, \end{aligned}$$

where λ is the eigenvalue of the stability analysis and λ_1 and λ_2 are its real and imaginary parts.

The simulations of (1) show that the onset of standing waves at the boundary to the stable homogeneous periodic solution is soft, and the standing wave is characterized by a

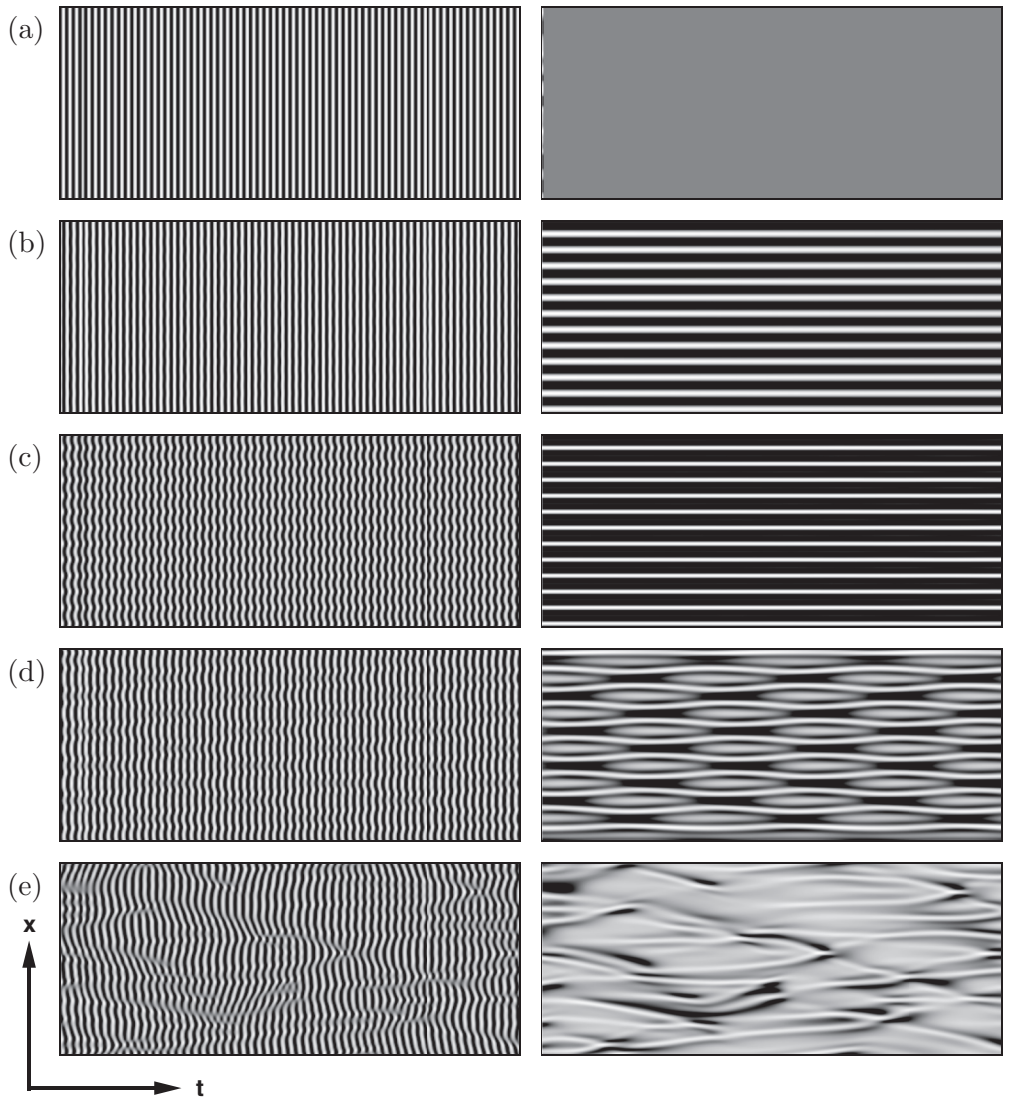

FIG. 1. Main spatiotemporal solutions for different feedback magnitudes. From uniform oscillations (a) via harmonic standing waves (b), period-2 standing waves (c), breathing standing waves (d), to spatiotemporal chaos (e). Shown are space-time diagrams in gray scale for ReA (left panels) and $|A|$ (right panels) for a time interval of $t = 50$ in the asymptotic regime. Due to the strong contribution of the uniform oscillations, the standing waves are difficult to recognize for ReA in (b) and (c), although they are clearly visible for $|A|$. Note that the period-2 behavior is in space (not in time) and is difficult to see due to the small amplitude but is clearly seen in Fig. 2. The parameters are $m_l = 0.7$, $m_g = 0.3$, $\tau = 0.3$. The values of μ are $\mu = 1.00$ (a), $\mu = 0.90$ (b), $\mu = 0.55$ (c), $\mu = 0.50$ (d), and $\mu = 0.44$ (e). Black (white) denotes low (high) values of the respective quantity (rescaled for each simulation). For $|A|$, these values are $(|A|_{\min},|A|_{\max}) = (0.753,0.753)$ (a), $(|A|_{\min},|A|_{\max}) = (0.744,0.762)$ (b), $(|A|_{\min},|A|_{\max}) = (0.636,0.953)$ (c), $(|A|_{\min},|A|_{\max}) = (0.57,0.98)$ (d), $(|A|_{\min},|A|_{\max}) = (0.15,1.1)$ (e). The other parameters are $\alpha = -1.4$, $\beta = 2$, $\omega = 2\pi - \alpha$, $\xi = \pi/2$. System size, $L = 128$.

vanishing space-dependent part at threshold [24]. Hence, by constructing a standing wave solution with nonzero amplitude, we are necessarily off threshold. However, then the uniform periodic solution is unstable not only to one critical wave number k_c, but to a band of wave numbers. Typically, the wave number observed in simulations in this case is the one which corresponds to the maximal growth rate $k_{\max}$, given by the condition $\partial_k \lambda_1(k_{\max}) = 0$ [where $\lambda_1(k_{\max}) > 0$].

Standing waves in this system arise as spatial modulations of the amplitude on top of the uniform oscillations; the ansatz is therefore

$$A(x,t) = H(t) + B_k(t)(e^{ikx} + e^{-ikx}), \tag{6}$$

with H being the uniform mode and B_k the complex amplitude of the mode with wave number k. This ansatz can also be interpreted as a rightgoing wave (with wave number k) and a leftgoing one (with wave number $-k$) sharing the same amplitude and thus describing a standing wave pattern.

Before inserting ansatz (6) into Eq. (1), we have to determine several terms appearing in Eq. (1), with

$$\begin{aligned} |A|^2 A = {} & |H|^2 H + 4|B_k|^2 H + 2H^* B_k^2 \\ & + (e^{ikx} + e^{-ikx})(H^2 B_k^* + 2|H|^2 B_k + 3|B_k|^2 B_k) \\ & + (e^{2ikx} + e^{-2ikx})\left(2H|B_k|^2 + H^* B_k^2\right) \\ & + (e^{3ikx} + e^{-3ikx})|B_k|^2 B_k, \end{aligned} \tag{7}$$

and

$$\begin{aligned} F_l &= \mu m_l e^{i\xi}\{[H(t-\tau)-H(t)] \\ &\quad +(e^{ikx}+e^{-ikx})[B_k(t-\tau)-B_k(t)]\}, \\ F_g &= \mu m_g e^{i\xi}[H(t-\tau)-H(t)]. \end{aligned} \tag{8}$$

being of particular relevance. Equation (8) assumes that the space-dependent part of $A(x,t)$ does not contribute to the average $\bar{A}(t)$. This is fulfilled if $L\to\infty$ or $L=2\pi n/k$ (with $n=1,2,\ldots$). In the following, we neglect the higher-order harmonic contributions in Eq. (7), which close to onset is well justified. Inserting finally ansatz (6) into Eq. (1), and using Eqs. (7) and (8), we obtain

$$\begin{aligned} &\frac{dH}{dt}+(e^{ikx}+e^{-ikx})\frac{dB_k}{dt} \\ &\quad=(1-i\omega)[H+(e^{ikx}+e^{-ikx})B_k] \\ &\qquad-(1+i\alpha)\big[|H|^2H+4|B_k|^2H+2H^*B_k^2 \\ &\qquad+(e^{ikx}+e^{-ikx})(H^2B_k^*+2|H|^2B_k+3|B_k|^2B_k)\big] \\ &\qquad-(1+\mathrm{i}\beta)k^2(e^{ikx}+e^{-ikx})B_k \\ &\qquad+\mu(m_l+m_g)e^{i\xi}[H(t-\tau)-H(t)] \\ &\qquad+\mu m_l e^{i\xi}[B_k(t-\tau)-B_k(t)](e^{ikx}+e^{-ikx}). \end{aligned} \tag{9}$$

Now we separate the equation into space-dependent and space-independent parts and arrive at

$$\begin{aligned} \frac{dH}{dt} &= (1-i\omega)H-(1+i\alpha)\big(|H|^2H+4|B_k|^2H+2B_k^2H^*\big) \\ &\quad+\mu(m_l+m_g)e^{i\xi}[H(t-\tau)-H(t)], \\ \frac{dB_k}{dt} &= (1-i\omega)B_k-(1+i\alpha)(H^2B_k^*+2|H|^2B_k+3|B_k|^2B_k) \\ &\quad-(1+i\beta)k^2B_k+\mu m_l e^{i\xi}[B_k(t-\tau)-B_k(t)]. \end{aligned} \tag{10}$$

In the case of $B_k=0$, the first equation reduces to the equation describing the mode of the homogeneous periodic solution. However, the coupling terms in the first equation of Eq. (10) tell us that if $B_k\neq 0$, the uniform mode H is different from the uniform oscillations (3) and we cannot use Eq. (4).

To solve Eq. (10), we assume the solution to be of the following form [27]:

$$\begin{aligned} H &= H_0 e^{-i\Omega_0 t}, \\ B_k &= B_{k0}e^{-i(\Omega_0 t+\gamma)}. \end{aligned} \tag{11}$$

Thus, both modes oscillate at the same frequency Ω_0, while there is a phase shift γ between the modes. The real amplitudes are given by H_0 and B_{k0}, respectively.

After inserting (11) into (10), we obtain

$$\begin{aligned} (-i\Omega_0)H &= (1-i\omega)H-(1+i\alpha)\big(H_0^2+4B_{k0}^2 \\ &\quad+2B_{k0}^2e^{-2i(\Omega_0 t+\gamma)}e^{2i\Omega_0 t}\big)H \\ &\quad+\mu(m_l+m_g)e^{i\xi}(e^{i\Omega_0\tau}-1)H, \\ (-i\Omega_0)B_k &= (1-i\omega)B_k-(1+i\alpha)\big(H_0^2e^{-2i\Omega_0 t}e^{2i(\Omega_0 t+\gamma)} \\ &\quad+2H_0^2+3B_{k0}^2\big)B_k-(1+i\beta)k^2B_k \\ &\quad+\mu m_l e^{i\xi}(e^{i\Omega_0\tau}-1)B_k. \end{aligned} \tag{12}$$

Dropping H from the first equation and B_k from the second, this simplifies to

$$\begin{aligned} 0 &= 1+i\Omega_0-i\omega-(1+i\alpha)\big(H_0^2+4B_{k0}^2+2B_{k0}^2e^{-2i\gamma}\big) \\ &\quad+\mu(m_l+m_g)e^{i\xi}(e^{i\Omega_0\tau}-1), \\ 0 &= 1+i\Omega_0-i\omega-(1+i\alpha)\big(H_0^2e^{2i\gamma}+2H_0^2+3B_{k0}^2\big) \\ &\quad-(1+i\beta)k^2+\mu m_l e^{i\xi}(e^{i\Omega_0\tau}-1). \end{aligned} \tag{13}$$

These equations can be separated into real and imaginary parts. We write them as

$$\begin{aligned} 0 &= 1-\big[H_0^2+2B_{k0}^2(2+\cos 2\gamma)\big] \\ &\quad-2\alpha B_{k0}^2\sin 2\gamma+\mu(m_l+m_g)\chi_1^s, \\ 0 &= \Omega_0-\omega-\alpha\big[H_0^2+2B_{k0}^2(2+\cos 2\gamma)\big] \\ &\quad+2B_{k0}^2\sin 2\gamma+\mu(m_l+m_g)\chi_2^s, \\ 0 &= 1-k^2-\big[H_0^2(2+\cos 2\gamma)+3B_{k0}^2\big] \\ &\quad+\alpha H_0^2\sin 2\gamma+\mu m_l\chi_1^s, \\ 0 &= \Omega_0-\omega-\beta k^2-\alpha\big[H_0^2(2+\cos 2\gamma)+3B_{k0}^2\big] \\ &\quad-H_0^2\sin 2\gamma+\mu m_l\chi_2^s, \end{aligned} \tag{14}$$

where $\chi_{1,2}^s$ are given by

$$\begin{aligned} \chi_1^s &= \cos(\xi+\Omega_0\tau)-\cos\xi, \\ \chi_2^s &= \sin(\xi+\Omega_0\tau)-\sin\xi. \end{aligned} \tag{15}$$

For a given k, Eqs. (14) can be solved numerically through root-finding algorithms, giving solutions for H_0, B_{k0}, Ω_0, and γ. There, the wave number k is provided by the eigenvalue problem studied in [25], where we use either k_c (at threshold) or $k_{\max}$ (away from threshold). Combining Eqs. (6) and (11), the family of standing wave solutions can be written as

$$A_{SW}=e^{-i\Omega_0 t}[H_0+2B_{k0}\cos(kx)e^{-i\gamma}]. \tag{16}$$

C. Numerical simulations and comparison to analytical solution

For numerical integration of Eqs. (1) in one-dimensional space, we choose the system size of $L=128$ with a spatial resolution of $\Delta x=0.32$. For time integration, we use an explicit Euler scheme with $\Delta t=0.002$. The Laplacian operator is discretized using a next-neighbor representation. We apply periodic boundary conditions and the initial conditions consist of developed spatiotemporal chaos. The overall simulation time for a given parameter set is $t=500$ (usually the systems reach the stable asymptotic state before $t=200$). For the sake of comparison with Refs. [24,25], the parameters are chosen as $\alpha=-1.4$, $\beta=2$, $\omega=2\pi-\alpha\approx 7.68$, $\xi=\pi/2$. Therefore, the Benjamin-Feir criterion $1+\alpha\beta<0$ is met and we observe amplitude turbulence in the absence of feedback. Although we do not vary m_l or m_g in this article, we keep $m_l+m_g=1$ constant as in [24,25].

As an example for standing waves, we choose $m_l=0.7$, $m_g=0.3$, $\mu=0.7$, and $\tau=0.3$. As result of simulation, we observe a standing wave with wave number $k=0.589$ and an amplitude profile $|A|$ shown in Fig. 2 as a black curve. Note that it actually shows a "period-2" behavior since we are

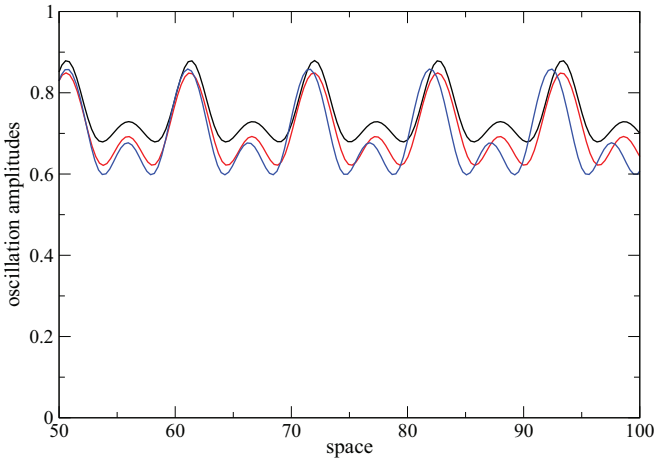

FIG. 2. (Color online) Amplitude profiles for $\mu = 0.7$ (other parameters as in Fig. 1). Shown are simulation [black curve (top curve at space point 55)], theoretical result using the theoretically obtained wave number [blue curve (bottom curve at 55)], theoretical result using the wave number observed in the simulations [red curve, central curve at 55]. We display only a part of the medium (total size, $L = 128$).

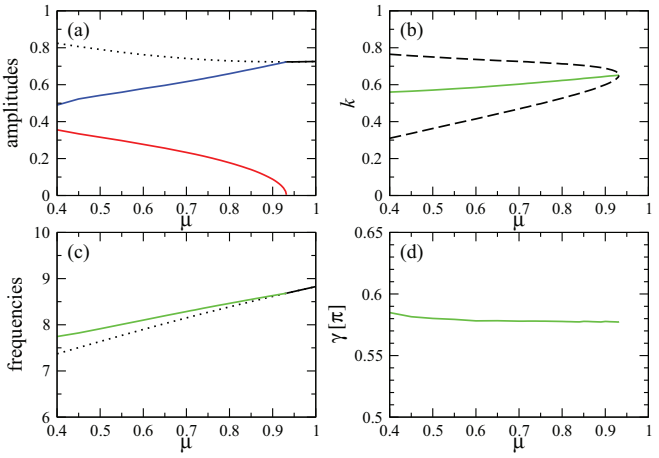

FIG. 3. (Color online) (a) Amplitudes H_0 (blue curve or upper gray curve) and B_{k0} (red or lower gray curve) of the standing waves and the amplitude ρ_0 of uniform oscillations (black) as function of μ. The dotted curve indicates the unstable uniform periodic solution. (b) Wave number k (green or gray) of the pattern as a function of μ at threshold $\mu_c = 0.932$, $k = k_c = 0.652$. For $\mu < \mu_c$, we show $k_{\max}$. Dashed black curves indicate the limits of k of the family of standing wave solutions. (c) Frequency Ω_0 of standing waves (green or gray curve) vs frequency Ω of uniform oscillations (black). The dotted curve corresponds to the unstable uniform oscillations. (d) Phase shift γ as function of μ (in multiples of π). Note that this figure only describes the solution itself, not its stability. Around $\mu \approx 0.5$, breathing sets in, and around $\mu \approx 0.4$, turbulence.

quite off threshold (for all other parameters fixed, the onset of standing waves occurs at $\mu_c = 0.932$). By nonlinear curve fitting, we obtain $(\Omega_0, H_0, B_{k0}, \gamma) = (8.11, 0.683, 0.213, 1.752)$ from the simulations. However, for the chosen parameter values, the stability analysis of uniform oscillation gives $k_{\max} = 0.603$ and the eigenvalue analysis (14) using this wave number yields $(\Omega_0, H_0, B_{k0}, \gamma) = (8.29, 0.616, 0.233, 1.816)$. The corresponding spatial amplitude profile is shown in Fig. 2 as a blue curve. Quantitative differences to the simulated pattern are close to 10% or smaller, and the amplitude profiles agree qualitatively very well. Taken into account that *both* stability analysis of uniform oscillations and analytical solution of standing waves use approximations like neglecting higher-order terms, the agreement can be considered very good. Furthermore, the simulations were carried out for a relatively small system and the periodic boundary conditions imply that we have an integer (and relatively small) number of waves in the system, in this case 12. Therefore, in general, it cannot be expected that the observed wave number (here $k = 0.589$) matches the wave number predicted by the stability analysis of uniform oscillations $k_{\max} = 0.603$. If we use $k = 0.589$ to calculate the standing wave solution through (14), we obtain $(\Omega_0, H_0, B_{k0}, \gamma) = (8.26, 0.636, 0.221, 1.786)$; i.e., all deviations become smaller and quantitative agreement improves (displayed as a red curve in Fig. 2).

D. Properties of standing waves

To analyze the onset of standing waves a little further, in Fig. 3(a) we show the amplitudes of the standing wave modes, the uniform one H_0 and the spatial one B_{k0} as function of μ. From the stability analysis of uniform oscillations [25], we obtain their amplitude ρ and the point where they become unstable: Here, the onset of standing waves occurs at $\mu_c = 0.932$, and the standing wave solution exists for μ smaller than μ_c. From that analysis, we also obtain $k_c = 0.652$ (at threshold) or $k_{\max}$ (away from threshold) that we use in Eq. (14) to calculate the properties of the standing waves. The values of k decrease as we move away from μ_c, but change less than 15% over the whole studied interval [Fig. 3(b)]. Within the area confined by dashed curves, standing wave solutions with a given k exist; i.e., the solution with $k = k_{\max}$ is just one possible representative of a family of solutions. We do not discuss the stability of these solutions here. Coming back to Fig. 3(a), we observe that the solution corresponding to uniform oscillations also exists for $\mu < \mu_c$, but is unstable. As expected, the amplitude B_{k0} increases as we move away from μ_c. Its magnitude shows a square root dependence as a function of the distance to the bifurcation point: $B_{k0} = 0.5(\mu_c - \mu)^{1/2}$. Note that the total amplitude of the space-dependent part in (16) is given by $2B_{k0}$; i.e., the total amplitude follows the typical square-root dependence from the bifurcation point. In Fig. 3(c), we see that the oscillation frequency of standing waves Ω_0 is larger than the oscillation frequency of the unstable uniform oscillations Ω. Both frequencies vary approximately linearly with μ (at least close to μ_c), and so does their difference. Finally, we also give the value of γ of the computed solution as a function of μ [Fig. 3(d)]. Note that this figure only describes the standing wave solution itself, not its stability. Around $\mu \approx 0.5$, breathing sets in, and around $\mu \approx 0.4$, turbulence.

E. Breathing standing waves

As we have seen in Fig. 1(d), we observe breathing standing waves, where, periodically, strong dips in the amplitude $|A|$ (noted as black areas in the right panel) are present. However, the amplitude maxima (right panel) also oscillate slightly

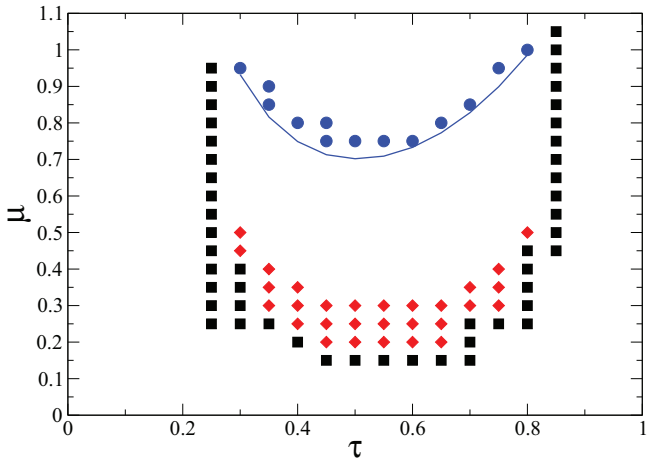

FIG. 4. (Color online) Stability area for the standing wave solution, as obtained by simulations where μ and τ were changed in steps of 0.05, respectively. Stable regular standing waves are found in the open center region, limited by developed turbulence (black squares), uniform oscillations (blue circles), and irregular (breathing) standing waves (red diamonds). The curve indicates the analytically calculated onset of standing waves. System size $L = 256$, other parameters are as in Fig. 1.

in space, and consequently the pattern could also be called "swinging" standing waves. In any case, the standing wave pattern is still clearly seen as the underlying pattern for ReA (left panel).

In Fig. 4, we show for the case $m_g = 0.7, m_l = 0.3$ the area where regular and breathing standing waves are found: Stable regular standing waves are found in the open center region, limited by developed turbulence (black squares), uniform oscillations (blue circles), and irregular (breathing) standing waves (red diamonds). We note that the breathing standing waves are observed far from onset of the regular standing waves. Indeed, we can perceive them as a transitory pattern to fully developed turbulence. To understand the onset of the breathing behavior in more detail, we performed simulations for $\tau = 0.3$, where μ was decreased in steps of 0.01 (starting from a stable standing wave pattern), and for different system sizes. We observed that for larger system sizes, the breathing set in for slightly *smaller* μ (simulations not shown). This can be explained by the fact that for a larger system size, the standing wave pattern that is formed in the stable regime can have a wave number closer to the optimal one, i.e., $k_{\max}$, whereas in a smaller system, the condition to have an integer number of waves forces the system to adopt a wave number farther away from $k_{\max}$ (this always assuming that the pattern with $k = k_{\max}$ is formed, excluding possible other pattern selection processes). While patterns with different k may coexist in general, it is obvious that their stability properties need not to be the same. In particular, patterns with different k can become unstable to breathing at different μ.

IV. CONCLUSION

In this article, we derived the solutions of standing waves for a CGLE in the presence of global and local time-delay feedback terms and studied their properties analytically and numerically. It is given by

$$A_{SW} = e^{-i\Omega_0 t}[H_0 + 2B_{k0}\cos(kx)e^{-i\gamma}], \tag{17}$$

where k is given by the eigenvalue problem studied in [25]; i.e., it corresponds either to k_c (at onset of the standing wave pattern) or $k_{\max}$ (away from onset) and H_0, B_{k0}, Ω_0, and γ calculated from (14).

The complex Ginzburg-Landau equation describes the dynamics of a spatially extended system that undergoes a supercritical Hopf bifurcation. The basic solution in this system corresponds to uniform oscillations. We considered the situation where this solution is Benjamin-Feir unstable in the absence of feedback ($1 + \alpha\beta < 0$), leading to spatiotemporal chaos. Then, uniform oscillations can be induced through the feedback. Standing waves are observed where this solution becomes unstable with respect to perturbations with a certain wave number [shown in Fig. 1(b)]. We have shown that analytical theory describes well the numerically observed properties of the pattern. We have illustrated this with an example even far from onset. Standing waves represent a family of solutions with different wave number k.

Standing waves can become unstable to a breathing mode. It can be interpreted as an intermediate stage between fully developed turbulence and regular standing waves, an effect that also depends on system size. No general stability analysis has been carried out for standing waves, but it is expected that solutions with different k have different stability properties (for all other parameters fixed).

Standing waves have been reported for a CGLE under global feedback without explicit time delay [27–30] and later also under global feedback with time delay [23]. To the best of our knowledge, an explicit solution of standing waves was first formulated in [27] [Eqs. (16) and (18)] and then in [30] [Eq. (6)]. However, in systems without time delay, more analytical results are available than in systems with time delay where the fundamental equations become delay differential equations and more results rely on numerical evaluation. Furthermore, in contrast to the above-mentioned studies, our model contains local feedback terms. According to the simulations and the stability analysis of uniform oscillations [25], local feedback terms enlarge the area where standing waves can be stabilized. So while local feedback is not necessary to produce standing waves, it is favorable. For purely local feedback, standing waves are observed even for low feedback magnitudes, while uniform oscillations then require high feedback magnitudes.

[1] M. C. Cross and P. C. Hohenberg, Rev. Mod. Phys. **65**, 851 (1993).
[2] I. S. Aranson and L. Kramer, Rev. Mod. Phys. **74**, 99 (2002).
[3] A. S. Mikhailov and K. Showalter, Phys. Rep. **425**, 79 (2006).
[4] E. Schöll and H. G. Schuster (eds.), *Handbook of Chaos Control* (Wiley-VCH, Weinheim, 2007).

[5] M. Kim *et al*., Science **292**, 1357 (2001).
[6] C. Beta, M. Bertram, A. S. Mikhailov, H. H. Rotermund, and G. Ertl, Phys. Rev. E **67**, 046224 (2003).
[7] V. K. Vanag, A. M. Zhabotinsky, and I. R. Epstein, J. Phys. Chem. A **104**, 11566 (2000).
[8] F. W. Schneider, E. Schöll, and M. A. Dahlem, Chaos **19**, 015110 (2009).
[9] D. J. Christini and L. Glass, Chaos **12**, 732 (2002).
[10] N. Baba, A. Amann, E. Schöll, and W. Just, Phys. Rev. Lett. **89**, 074101 (2002).
[11] J. Unkelbach, A. Amann, W. Just, and E. Schöll, Phys. Rev. E **68**, 026204 (2003).
[12] M. Stich, C. Punckt, C. Beta, and H. H. Rotermund, Philos. Trans. R. Soc., A **366**, 419 (2008).
[13] M. E. Bleich and J. E. S. Socolar, Phys. Rev. E **54**, R17 (1996).
[14] I. Harrington and J. E. S. Socolar, Phys. Rev. E **64**, 056206 (2001).
[15] K. A. Montgomery and M. Silber, Nonlinearity **17**, 2225 (2004).
[16] C. M. Postlethwaite and M. Silber, Physica D **236**, 65 (2007).
[17] V. García-Morales and K. Krischer, Phys. Rev. Lett. **100**, 054101 (2008).
[18] V. García-Morales and K. Krischer, Phys. Rev. E **78**, 057201 (2008).
[19] V. García-Morales, A. Orlov, and K. Krischer, Phys. Rev. E **82**, 065202(R) (2010).
[20] T. Erneux, *Applied Delay Differential Equations* (Springer, New York, 2009).
[21] K. Pyragas, Phys. Lett. A **170**, 421 (1992).
[22] A. C. Casal and J. I. Díaz, Math. Models Methods Appl. Sci. **16**, 1 (2006).
[23] C. Beta and A. S. Mikhailov, Physica D **199**, 173 (2004).
[24] M. Stich, A. C. Casal, and J. I. Díaz, Phys. Rev. E **76**, 036209 (2007).
[25] M. Stich and C. Beta, Physica D **239**, 1681 (2010).
[26] M. Stich and C. Beta, Discrete Contin. Dyn. Syst. Suppl. **2011**, 1329 (2011).
[27] M. Falcke, H. Engel, and M. Neufeld, Phys. Rev. E **52**, 763 (1995).
[28] F. Mertens, R. Imbihl, and A. Mikhailov, J. Chem. Phys. **101**, 9903 (1994).
[29] D. Battogtokh and A. Mikhailov, Physica D **90**, 84 (1996).
[30] D. Lima *et al*., Europhys. Lett. **42**, 631 (1998).